Carbon 109 (2016) 874–882

Contents lists available at ScienceDirect

Carbon

journal homepage: www.elsevier.com/locate/carbon

Graphite oxide paper as a polarizable electrical conductor in the through-thickness direction

Xinghua Hong [a, b], Weidong Yu [b], Andi Wang [a], D.D.L. Chung [a, *, 1]

[a] Composite Materials Research Laboratory, Department of Mechanical and Aerospace Engineering, University at Buffalo, State University of New York, Buffalo, NY, 14260-4400, USA
[b] Key Laboratory of Textile Science & Technology, Ministry of Education, College of Textiles, Donghua University, Shanghai, 201620, China

ARTICLE INFO

Article history:
Received 18 July 2016
Received in revised form
16 August 2016
Accepted 26 August 2016
Available online 27 August 2016

ABSTRACT

Graphite oxide (GO) paper is a polarizable electrical conductor in the through-thickness direction, as shown by alternating-current electrical testing performed with decoupling of the volumetric and interfacial contributions. The solid part (69 vol%) of the dark brown paper (112–358 μm thick) exhibits carbon/oxygen atomic ratio 2.0, and interlayer spacing 8.60 Å. At 50 Hz and 2 MHz respectively, the in-plane conductivity is 0.07 and 2.5 S/m, the through-thickness conductivity is 6.7×10^{-6} and 4.8×10^{-3} S/m, the through-thickness relative dielectric constant is 915 and 91, the specific capacitance of the interface with an electrical contact is 18.3 and 1.1 μF/m^2, and the areal resistivity of this interface is 1.5×10^5 and 1.0×10^2 Ω cm^2. The conductivity is due to slightly incomplete intercalation (but without residual graphite), as shown by a weak X-ray diffraction peak at interlayer spacing 4.33 Å. The interface contributes, but the volumetric capacitance/resistance dominates. The decrease of κ with increasing frequency (50–200 Hz) is attributed to the functional-group-related dipole friction. The increase of the through-thickness conductivity with increasing frequency is attributed to the decreasing excursion of the charge carriers and the consequent decrease in the chance of the carriers to encounter interfaces.

1. Introduction

Electrical conduction involves the movement of charge carriers in response to an applied electric field. It is needed for numerous devices, including microelectronics, electrochemical devices (including batteries, supercapacitors and electrochemical gas sensors), pacemakers, etc., and is commonly provided by metals that are high in the electrical conductivity. Electric polarization pertains to the dielectric behavior and involves the separation of the positive and negative charge centers in a material in response to an applied electric field. Polarization is needed for dielectric capacitors, ferroelectric memories, piezoelectric devices (sensors, actuators, energy harvesters, etc.), electrostrictive devices, pyroelectric devices, and electrorheological fluids, and is commonly provided by ceramics and, to a lesser degree, polymers. Due to its high conductivity, metals are not polarizable. Due to their low electrical conductivity, ceramics and polymers are typically inadequate electrical conductors.

Polarizable electrical conductors are conductors that are intermediate in the conductivity, so that they can provide both electrical conduction and polarization. Such a combination of dielectric and conduction behavior is valuable for electromagnetic interference (EMI) shielding [1], the mechanisms of which can involve the interaction of the electromagnetic radiation with the charge carriers as well as the interaction of the radiation with the electric dipoles in the material. Polarizable electrical conductors are also valuable as optoelectronic materials, as needed for electrical-to-optical and optical-to-electrical transducers, solar cells, phototransistors and integrated optical circuits. Furthermore, polarizable electrical conductors can be valuable as catalysts, since the catalysis can involve both conduction and dielectric mechanisms.

Carbon in the form of graphite is an electrical conductor, due to the sp^2 hybridization and the in-plane delocalization of its $2p_z$ electrons [2]. In contrast, carbon in the form of diamond is an electrical insulator, due to the sp^3 hybridization and the covalent bonding. Thus, a suitable combination of sp^2 and sp^3 hybridization in modified carbons can provide a route for obtaining polarizable electrical conductors.

* Corresponding author.
E-mail address: ddlchung@buffalo.edu (D.D.L. Chung).
[1] http://alum.mit.edu/www/ddlchung.

http://dx.doi.org/10.1016/j.carbon.2016.08.083
0008-6223/

In graphite oxide (abbreviated GO and also known as graphitic acid), the covalent bonding stems from the presence of conjugated double bonds within the carbon planes. The layer planes assume a wavy form because of the change of the carbon bonding from the trigonal (sp^2) form to the tetrahedral (sp^3) form. Thus, GO is much less conductive than graphite, with an electrical conductivity that depends on the oxygen content. The GO retains the layer structure of graphite, but it has a much larger and less regular interplanar spacing.

Due to the relatively easy separation of the somewhat puckered topography of its atomic layers, GO can be easily exfoliated through dispersion in water, thereby forming stacks (flakes) with about 10 carbon layers or less per stack. Such stacks are also known as graphene oxide. As the chemical reduction of GO forms graphite, the dispersed GO is a widely used precursor for graphene [3,4]. Upon drying the GO dispersion, GO is obtained, either in particulate or paper form. The paper form refers to the sheet obtained after settlement of the GO at the bottom of the dispersion. The particulate form is attractive for use as a filler in composite materials, whereas the paper form is attractive for direct use. This work is focused on the paper form and does not address GO composites. Applications of GO include catalysis, sensor, supercapacitors, water purification, hydrogen storage and magnetic shielding, etc. [5–8].

The dielectric behavior of a material is mainly described by the relative dielectric constant (i.e., the relative permittivity), which relates to the volumetric capacitance and to the polarizability of the material. It is also described by the areal capacitance of the interface between the material and an electrical contact, which is necessarily involved in both research and application. In particular, the application as an electrode involves the making of an electrical contact to the electrode. The electrical conduction behavior of a material is mainly described by the electrical conductivity, which relates to the volumetric electrical resistance. It is also described by the areal resistance of the interface between the material and an electrical contact. All of the four quantities mentioned above tend to depend on the frequency. In spite of the relevance of the dielectric and electrical conduction behavior and the associated frequency dependence to supercapacitor applications [9], such behavior of GO has received little previous attention. Although the volumetric quantities have been reported, the areal quantities associated with the interface have not been previously reported. Furthermore, the relative dielectric constant that has been previously reported in the through-thickness direction of GO paper was determined by assuming that the interface contribution is negligible [10]; as a consequence, the accuracy of the reported relative dielectric constant is questionable. Although limited values of the electrical conductivity have been previously reported, the values reflect differences in the measurement method (which governs whether the volumetric and interfacial contributions are decoupled or not) and the measurement direction (i.e., the in-plane or through-thickness direction of the GO paper), and a clear picture cannot be obtained regarding the volumetric and interfacial contributions for either direction of measurement [11–14]. In particular, prior work on the measurement of the through-thickness conductivity and dielectric constant of GO paper used the two-probe method, so that the measured resistance includes the contact resistance and the measured capacitance includes the contact capacitance. As the specimen and the electrical contacts are electrically in series, this results in under-estimation of both the conductivity and the relative dielectric constant [12,14]. Since the contribution by the electrical contacts can be significant, the extent of under-estimation can be large.

Due to the fact that GO paper is not 100% dense, the dielectric and electrical conduction properties of the solid part of a GO paper (i.e., with the air excluded) must be distinguished from those of the overall paper (with the air included). The decoupling of the solid and air contributions was not made in previous work [10–14]. This decoupling is necessary for determining the properties of the GO solid in the paper.

This work is aimed at providing detailed information on the dielectric and electrical conduction behavior of GO paper, with emphasis on the behavior in the through-thickness direction. The approach is special in that it involves (i) decoupling the volumetric and interfacial contributions, with the interface being that between the GO paper and an electrical contact, (ii) decoupling the GO solid and air contributions, and (iii) studying the frequency dependence. The study has resulted in the discovery that GO is a polarizable electrical conductor in the through-thickness direction.

X-ray diffraction (XRD) is a basic technique for analyzing the structure of GO. According to the XRD results, three types of GO have been reported in prior work. Type I has the main XRD peak at 2θ ranging from 11 to 16° (CuKα radiation), with no graphite 002 peak [15–18]. Type II has the same main peak and, in addition, a weak peak at 2θ ranging from 18 to 21°, with no graphite 002 peak [19–23]. Type III has the same main peak, and, in addition, a weak graphite 002 peak at 26° [24,25]. The interpretation of the XRD results indicates that Type I is pure GO, Type II is GO with incomplete intercalation but no residual graphite, and Type III is GO with residual graphite. This work addresses Type II. The comparison of the electrical behavior of the three types of GO is beyond the scope of this work.

2. Experimental methods

The approach used for achieving the decoupling mentioned in Sec. 1 involves (i) measuring the through-thickness resistance and capacitance of the GO paper (for determining the quantities pertaining to the GO solid), and (ii) conducting the measurement for three GO paper thicknesses, thereby decoupling volumetric and cotmpact-contact interfacial quantities. The approach is the same as that of the prior work of two of the authors [26,27]. The prior work concerns graphite or carbon materials, such as exfoliated graphite [28], graphite nanoplatelet, carbon black and activated carbon. Please refer to the prior work [27] for the details of the testing set-up.

2.1. Materials

The graphite raw material for preparing the GO is Micro 850 from Asbury Graphite Mills, Inc. (Asbury, NJ). It is natural crystalline graphite with particle size 5 μm and 99% carbon. The GO is prepared using the modified Hummers method [29]. This method involves (i) putting 22.50 g of 98% sulfuric acid (H_2SO_4) and 0.500 g of sodium nitrate ($NaNO_3$) powder in an open glass beaker, followed by placing the beaker in a basin of ice water for the purpose of cooling the beaker 0 °C, (ii) adding 1.000 g of graphite, followed by magnetic stirring for 30 min, while the beaker remains cooled, (iii) slowly adding 3.000 g potassium permanganate ($KMnO_4$), while the beaker remains cooled, (iv) allowing the beaker to be heated naturally (due to the exothermic reaction) to 35 °C, which is kept for 30 min while magnetic stirring takes place, with the color changing from black to dark purplish green, (v) continuing the magnetic stirring for 2 days, with the color of the dispersion changing to dark brown, (vi) slowly adding 45 ml of de-ionized water, while stirred occurs, in order to prevent violent effervescence, thereby causing the temperature to increase to 90–95 °C, which is then maintained for 15 min, (vii) adding 10.00 ml of 30% hydrogen peroxide (H_2O_2) and 53.00 ml of deionized water in order to reduce the residual potassium permanganate and manganese dioxide (MnO_2) to form soluble manganese sulfate ($MnSO_4$), with

the color of the solid (GO) changing to bright yellow (characteristic of the maximally oxidized product with C:O ratio between 2.1 and 2.9 [13]), while the liquid above it is colorless, and (viii) drying the dispersion to obtain the solid (GO), which is dark brown.

The GO paper is prepared from the GO by (a) magnetically stirring the GO aqueous dispersion for 2 h, followed by allowing the dispersion to sit for 24 h for the purpose of having the GO settle down, then decanting the upper colorless water above the GO, and then adding hydrochloric acid (HCl) in the amount of 5% of the weight of the dispersion, followed by allowing the settling for 24 h and then decanting the colorless water above the GO, and then repeating all of step (a) once, (b) repeating again and again all of step (a), but using deionized water instead of hydrochloric acid until the decanted liquid has a pH close to 7, (c) sonicating thrice, with each time lasting 1.5 h, such that the color changes from bright yellow solid (before step (a)) to dark brown dispersion (after step (c)), (d) casting the dispersion into 50 × 50 mm square silicone molds with mold cavities of three different thicknesses, and then drying at room temperature for 72 h, followed by oven drying at 60 °C for 6 h. In order to remove moisture, the specimens are heated at 60 °C for 3 h immediately prior to electrical testing.

2.2. Electrical characterization methods

This work uses a technique which differs greatly from the widely used technique of electrochemical impedance spectroscopy (EIS). Firstly, it does not measure the impedance, but measures the relative permittivity (real part of the permittivity) and the conductivity (real part of the conductivity). Secondly, in relation to both permittivity and conductivity measurements, the technique of this work decouples the contribution of the specimen-contact interface from the contribution of the volume of the specimen. Thirdly, the technique of this work uses an equivalent circuit model (Fig. 1) that reflects the testing configuration, which entails two electrical contacts sandwiching the specimen (thus the contacts and the specimen are electrically in series), with each element in the configuration being modeled as a resistance and a capacitance in parallel. Furthermore, the circuit model reflects the material structure, which consists of carbon and air, which are assumed to be in parallel electrically. Fourthly, the technique of this work does not emphasize the frequency dependence of the permittivity or conductivity. In contrast, EIS emphasizes the frequency dependence of the impedance, as conventionally described in terms of the Nyquist plot, for the purpose of deriving by mathematical fitting of the plot an equivalent electrical circuit that describes the electrical/dielectric behavior of the material. Furthermore, EIS does not provide the abovementioned decoupling, so the obtained electrical parameters as well as their frequency dependence may be flawed. In addition, EIS involves a different testing configuration, which entails two electrodes (an anode and a cathode) separated by an electrolyte, i.e., the configuration of an electrochemical cell. Thus, the technique of this work provides different information from EIS. The technique of this work allows investigation in the material level, whereas EIS allows investigation in the electrochemical cell level.

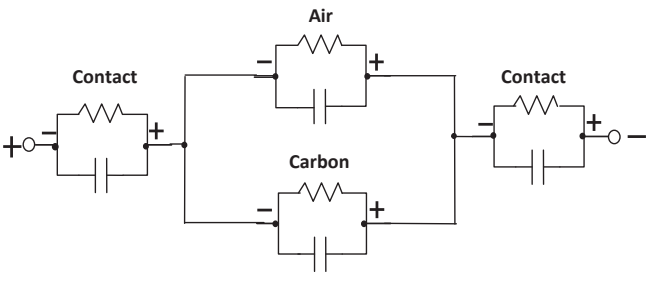

Fig. 1. Equivalent circuit model for the through-thickness electrical behavior of GO paper. The contact refers to the interface between the paper and an electrical contact.

In the technique of this work, the measurement of the real part of the relative permittivity is made possible by the presence of an electrically insulating polymer film at the interface between the specimen and each of the two copper electrical contacts and the performance of the measurement at three specimen thicknesses (along with the data analysis that concerns the slope of the plot of the reciprocal of the capacitance vs. the thickness) so as to decouple the contribution of the specimen-contact interface (with the contact including the film) from the contribution of the volume of the specimen. Due to the conductivity of the specimen, the presence of the film is important for ensuring that the real part of the permittivity is measured. On the other hand, the film is absent for the measurement of the conductivity. Similar conductivity measurement conducted at three specimen thicknesses enables the decoupling of the contribution of the specimen-contact interface from the contribution of the volume of the specimen.

Unless noted otherwise, the reported results are for the through-thickness direction. For both through-thickness and in-plane electrical measurements, specimens at three thicknesses are tested. The three thicknesses are 0.112 ± 0.003 mm, 0.244 ± 0.003 mm, and 0.358 ± 0.003 mm, correspond to specimen masses of 68.28 ± 0.01 mg, 148.22 ± 0.01 g and 216.69 ± 0.01 mg, respectively.

Each specimen for through-thickness dielectric/conductivity testing is a square with dimension 20.00 ± 0.10 mm at each edge of the square, as obtained by cutting and removing the four edge regions from the molded 50 × 50 mm square specimen.

Each specimen for in-plane electrical conductivity testing is a rectangular strip of width 4.840 ± 0.003 mm, and length exceeding 30.000 mm. The four-probe method is used, with the two inner voltage contacts being 19.200 ± 0.003 mm apart and two outer current contacts being 28.000 ± 0.003 mm apart. All four contacts are made with silver paint in conjunction with copper wires.

Please refer to our prior work [27] for the details in the through-thickness testing set-up. The only difference in the set-up from the prior work is that no frame is used in this work for holding the specimen, which is in the form of a standalone film and does not need a holder. The prior work [26,27] used a frame to hold the specimen, as necessitated by the fact that the specimen was in particle form. The specimen area is 20 × 20 mm in both this work and the prior work.

Fig. 1 shows the equivalent circuit used in this work for modeling the through-thickness conduction and dielectric behavior. In this circuit, carbon (the GO solid in the paper) and air (the pores in the GO paper) are electrically in parallel and this parallel combination is in series with both electrical contacts, which are in contact with the two opposite surfaces of the GO paper, thereby sandwiching the paper. All the quantities shown in the model are decoupled and determined using the method of prior work [26,27].

The through-thickness relative dielectric constant (which describes the volumetric dielectric behavior of the paper), the specific interfacial capacitance (which is the capacitance per unit area of the interface between the paper and either electrical contact), the through-thickness electrical resistivity (which describes the geometry-independent through-thickness volumetric conduction behavior of the paper) and the interfacial electrical resistivity (which is the geometry-independent areal resistivity of the interface between the paper and either electrical contact) are measured in this work, using a precision RLC meter (Quadtech 7600), with the

frequency ranging from 50 Hz to 2 MHz. The capacitance and resistance for the parallel RC circuit configuration are separately obtained from the meter, such that the capacitance is measured with an electrically insulating paper (thickness 75 μm) between the paper and each electrical contact and the resistance is measured without this insulating paper [26,27]. The use of the electrically insulating paper in case of capacitance measurement is for the purpose of minimizing the through-thickness current, thereby determining essentially the real part of the relative dielectric constant. The AC voltage is adjusted so that the electric field is fixed at 22.6 V/cm while the thickness varies, so the voltage is 0.50, 0.90 and 1.26 V for the three thicknesses.

In order to decouple the volumetric and interfacial contributions to the capacitance, specimens of three different thicknesses are tested. The electric field is applied between the two copper foils (thickness 62 μm), which are the electrical contacts. The pressure provided by a copper foil and a steel weight (above the foil) on the paper during testing is 4.3 kPa (0.63 psi). The decoupling of the contribution of the solid part of the paper and the air contribution is performed by using the Rule of Mixtures, with solid and air modeled as being electrically in parallel (Fig. 1) [27].

The volumetric capacitance of the paper (C_v) and the capacitance of the interface between the paper and an electrical contact (C_i) are in series, so the measured capacitance C is given by

$$1/C = 2/C_i + 1/C_v. \quad (1)$$

The factor of 2 in Eq. (1) is due to the presence of two interfaces on the two sides of the paper. Due to Eq. (1), C_i is less influential when it is large. The C_v is given by

$$C_v = \varepsilon_0 \kappa A/l, \quad (2)$$

where ε_0 is the permittivity of free space (8.85×10^{-12} F/m), κ is the through-thickness relative dielectric constant of the paper, A is the paper area (20.0×20.0 mm^2), and l is the paper thickness. The κ is the same as the real part κ' of the relative dielectric constant.

Due to Eqs. (1) and (2), the plot of $1/C$ against l is a straight line with the intercept of $2/C_i$ at the $1/C$ axis at $l = 0$, and the value of κ is obtained from the slope, which is equal to $1/(\varepsilon_0 \kappa A)$. The specific interfacial capacitance of the overall paper is the product of C_i and A; that of the RGO in the paper is the product of C_i and the part of A that is occupied by the RGO (rather than air). The fraction of A that is occupied relates to the porosity of the paper and is taken as the volume fraction of solid in the paper.

The measured resistance R between the two copper contacts that sandwich the paper includes the through-thickness volume resistance R_v of the paper and the resistance R_i of each of the two interfaces between the paper and a copper contact, i.e.,

$$R = R_v + 2R_i. \quad (3)$$

By measuring R at three paper thicknesses, the curve of R versus thickness is obtained. The intercept of this curve with the R axis at zero thickness equals $2R_i$, whereas the slope of this curve equals R_v/l, where R_v is the paper resistance for the paper thickness of l. The through-thickness paper resistivity is obtained by multiplying R_v/l by the specimen area A. The paper conductivity is the inverse of the paper resistivity. The areal resistivity of the interface between the paper and an electrical contact equals the product of R_i and A; that of the interface between the RGO in the paper and an electrical contact equals the product of R_i and the part of A that is occupied by the RGO (rather than air).

3. Results and discussion

3.1. Structure of the GO paper

The GO paper is dark brown in color. With the true density of GO taken to be 2.200 g/cm^3 [30], the solid content in the GO paper is found to be (69.03 ± 0.25) vol%. The GO paper is highly flexible.

The elemental composition of the paper, as determined by energy dispersive x-ray spectroscopy in conjunction with scanning electron microscopy, is shown in Table 1. The carbon/oxygen atomic ratio is 1.95 ± 0.23. This ratio, and the atomic concentrations of C and O are all close to those of prior work on GO [31]. The minor amount of sulfur (2.43 ± 0.40 at.%) is attributed to the sulfuric acid used in the GO preparation.

The diffraction pattern of graphite powder gives the 002 graphite diffraction peak at $2\theta = 26.44°$ that corresponds to an interlayer spacing of 3.38 Å (Fig. 2(a)). XRD of the GO paper (Fig. 2(b)) shows the main peak at $2\theta = 10.28°$. This corresponds to an interlayer spacing of 8.60 Å. The amount of adsorbed moisture affects the interlayer spacing of GO [32], so there is variability in the interlayer spacing among different published works. In addition, Fig. 2(b) shows a weak broad peak at 20.5° corresponding to an interlayer spacing of 4.33 Å. The weak peak has been previously reported in GO with C/O ratio 2.47 and interpreted as being due to the incomplete intercalation of a minor part of the material [19]. However, the absence of a graphite 002 peak in Fig. 2(b) indicates the absence of residual graphite.

Fig. 2(c) shows the Raman spectrum of the GO paper after vacuum drying at 60 °C for 24 h. The G and D peaks are comparable in intensity and are both quite broad, with the G peak narrower than the D peak. The area ratio of D-band intensity to G-band intensity of the GO paper is 1.004 ± 0.003. These features are similar to those of prior work [33].

Fig. 2(d) shows the Fourier-transform infrared reflection (FTIR) spectrum of the GO paper after vacuum drying at 60 °C for 24 h. The spectrometer is Nicolet 6700, Thermo Electron Corporation. The spectrum is similar to that of prior work on GO [20]. The overlapped bands in the 3700-2300 cm^{-1} correspond to the stretching vibrations of structural OH groups and water molecules. The broad OH bands of the spectrum may partly come from the high and strongly bound humidity content of GO [34]. The next peak around 1716 cm^{-1} corresponds to the C═O stretching of COOH groups located at the edges of the oxidized graphite [35]. The peak situated at 1574 cm^{-1} relates to the HOH bending vibrations of water [34]. The peaks at around 1150 cm^{-1}, 1034 cm^{-1} and 863 cm^{-1} correspond to different motions of the oxygenated groups (C–O stretching, C–O–H bending, C–O–C symmetric and asymmetric stretching) [34–36].

Scanning electron microscopy shows that the cross-sectional plane of the GO paper is lamellar in microstructure. The lamellar structure is in the form of corrugated sheets that are preferably oriented parallel to the plane of the paper. Transmission electron microscopy shows that the thickness of the exfoliated GO particles obtained after drying the GO dispersion is 0.01 μm or less. With the interlayer spacing of 8.60 Å, this thickness corresponds to the

Table 1
The elemental composition of GO, as determined by x-ray energy-dispersive spectroscopy.

Element	Wt.%	At.%	C/O atomic ratio
C	56.09 ± 1.98	64.52 ± 2.14	1.95 ± 0.23
O	38.26 ± 2.81	33.04 ± 2.49	
S	5.65 ± 0.92	2.43 ± 0.40	

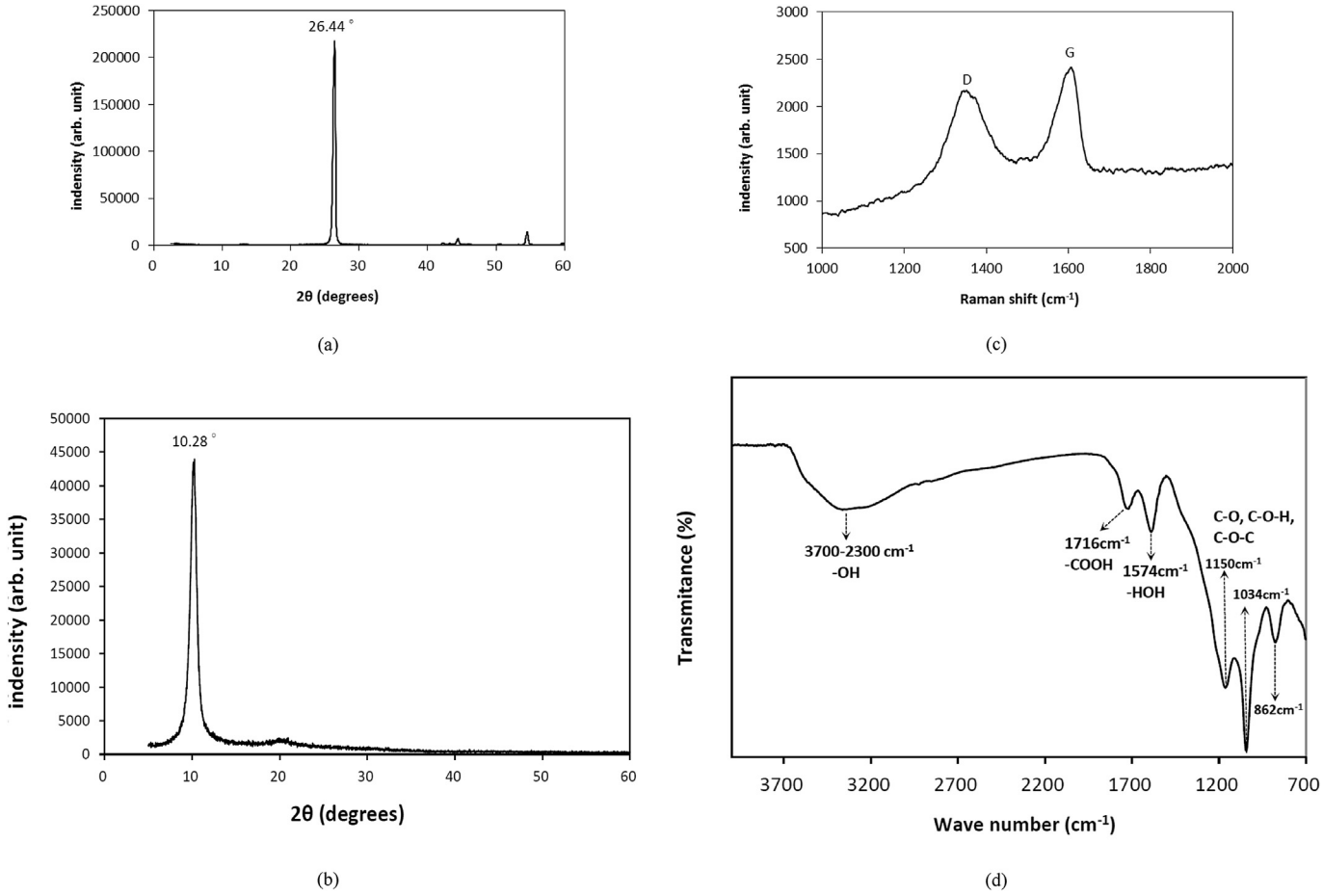

Fig. 2. X-ray diffraction (XRD) and Fourier-transform infrared (FTIR) spectroscopy results. (a) XRD pattern of graphite powder. (b) XRD pattern of GO paper. (c) Raman spectrum of GO paper. (d) FTIR spectrum of GO paper.

presence of ≤12 carbon layers in an exfoliated GO particle.

Fig. 3 shows representative plots of the resistance vs. paper thickness and of the reciprocal of the capacitance vs. paper thickness respectively. The strong linearity of all the plots in Fig. 3 is consistent with Eqs. (1) and (3) and supports the validity of this work's approach for decoupling of the volumetric and interfacial contributions.

3.2. Electrical testing results of the GO paper

Fig. 4(a) and (b) show that the through-thickness relative dielectric constant. The highest value is 632 and 915 for the GO paper (with air included) and the solid part of the paper (with air excluded), respectively, both obtained at the lowest frequency of 50 Hz (Fig. 4(a)). At the highest frequency (2 MHz) studied, the solid part of the paper exhibits relative dielectric constant 91 only (Fig. 4(b)). These values are all high and are attributed to the functional groups, which result from the oxidation of the graphite and are known to be abundant for GO. The functional groups on GO include epoxy bridges and pairwise carboxyl groups [37], the coordinated chemical structures of which hinder the movement of the functional groups. The values are comparable to those of exfoliated graphite that has not been washed by water to remove the residual acidity [26] and are much higher than those of exfoliated graphite that has been washed [27].

The through-thickness relative dielectric constant decreases with increasing frequency, as expected. The decrease is particularly abrupt in the low frequency regime from 50 Hz to 10 kHz. Above 10 kHz, the relative dielectric constant essentially levels off (at a value around 100 for the GO solid) up to the highest frequency of 2 MHz. The trend is the same for both the overall paper (with air included) and the solid part of the paper (with air excluded). This trend is attributed to the dipole friction associated with the abovementioned functional groups on the GO.

Fig. 4(c) shows that the specific contact capacitance of the paper-contact interface decreases with increasing frequency, with the decrease occurring mainly in the low frequency range up to 10 kHz. The values range from 18.3 $\mu F/m^2$ at the lowest frequency of 50 Hz to 1.11 $\mu F/m^2$ at the highest frequency of 2 MHz. These values are higher than those of natural graphite, carbon black and exfoliated graphite [27]. In view of Eq. (1), this means that the interface for GO does not influence the measured capacitance as much as the corresponding interface for these other carbons. Nevertheless, the interface for GO still contributes substantially to the measured capacitance, as quantified below.

Fig. 5(a) shows that the through-thickness AC conductivity of the GO paper increases with increasing frequency, such that the increase is more significant at frequencies above 10 kHz than frequencies below 10 kHz. The conductivity ranges from 6.7×10^{-6} S/m at the lowest frequency of 50 Hz to 4.8×10^{-3} S/m at the highest frequency of 2 MHz. These values are lower than those of conventional carbon fibers by 11 orders of magnitude [38]. They are

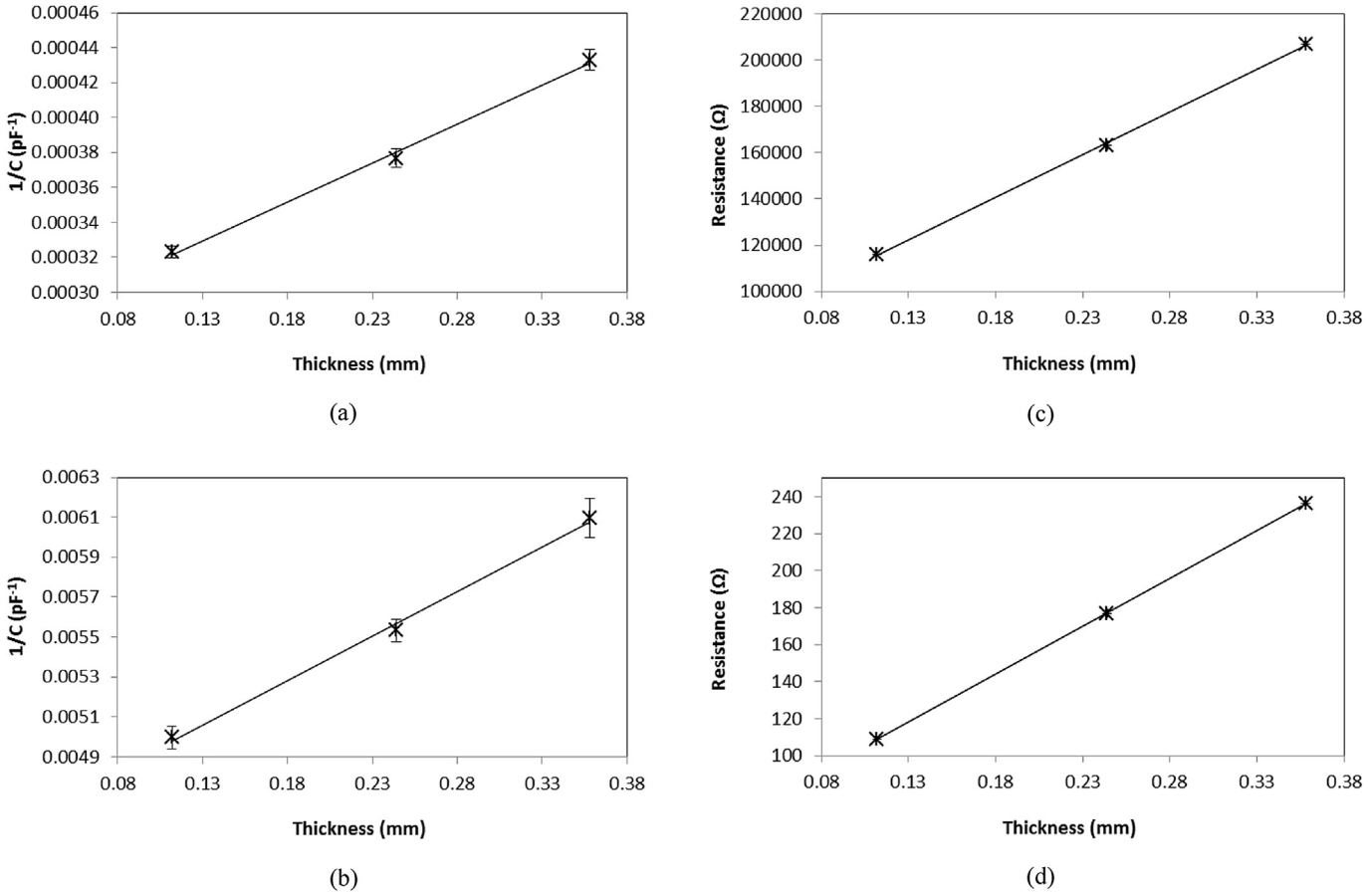

Fig. 3. (a–b) Plot of $1/C$ (where C is the measured capacitance) vs. the GO paper thickness (three different thicknesses) for the determination of the through-thickness relative dielectric constant. The error bars are shown, though they are too short to be clearly shown in (b). (a) 50 Hz. (b) 2 MHz. (c–d) Plot of the measured through-thickness resistance R vs. the specimen thickness for GO paper of three different thicknesses. The error bars are shown, though they are too short to be shown clearly. (c) 50 Hz. (d) 2 MHz.

also lower than those of exfoliated graphite or carbon black by 7 orders of magnitude [27]. Nevertheless, the conductivity is higher than those of insulators by at least several orders of magnitude, due to the sulfur-containing and oxygen-containing functional groups (Table 1 and Fig. 1).

The abovementioned frequency dependence of the through-thickness conductivity is attributed to the decreasing excursion of the charge carriers in a cycle as the frequency increases and the consequent decrease in the chance of the carriers to encounter an interface, such as the interface between adjacent exfoliated GO particles or flakes (with each particle or flake being essentially a stack of a few carbon layers). Since the relevant conductivity is in the through-thickness direction of the GO paper, there are numerous inter-particle interfaces along the thickness of the paper and the carriers can encounter these interfaces as they move in response to the applied electric field. Due to the relatively high resistance at each of these interfaces, the less that the carriers encounter interfaces, the greater is the conductivity.

Fig. 5(b) shows the areal resistivity of the interface between the GO paper and an electrical contact. This resistivity decreases with increasing frequency, such that the decrease is more significant above 10 kHz. In general, the resistivity of an interface tends to be lower when the materials of the proximate surfaces that come together to form this interface are more conductive. Therefore, the trend of the interfacial resistivity in Fig. 5(b) is consistent with the trend of the volumetric conductivity in Fig. 5(a). The interfacial resistivity of the solid part of the paper ranges from $1.5 \times 10^5\ \Omega\ cm^2$ at the lowest frequency of 50 Hz–$1 \times 10^2\ \Omega\ cm^2$ at the highest frequency of 2 MHz. These values may be acceptably low for electrochemical applications, though the acceptability depends on the specific dimensions, which strongly affect the capacitance. Nonetheless, these values suggest that the interfacial resistance cannot be ignored.

Fig. 6(a) shows that, for the paper dimensions of this work, C_i is higher than C_v by a factor of 2–3, meaning that the interfacial capacitance contributes substantially to the measured capacitance, though the volumetric capacitance dominates. The ratio of C_i–C_v is essentially independent of the frequency. The greater is the thickness, the higher is the ratio. This is because a greater thickness is associated with a lower volumetric capacitance.

Fig. 6(b) shows that, for the paper dimensions of this work, the ratio of R_i to R_v is below 0.35, meaning that R_i contributes to the measured resistance, though R_v dominates. The ratio is quite independent of the frequency up to 10 kHz. The smaller is the thickness, the greater is the ratio. This is because a smaller thickness is associated with a lower through-thickness volumetric resistance.

Prior work reported a through-thickness conductivity of 10^{-6} S/m and a through-thickness relative dielectric constant of 3 at 100 Hz and 30 °C for a GO paper of thickness 3 μm [14]. In contrast, by decoupling the volumetric and interfacial contributions, this work obtains a conductivity of 9×10^{-6} S/m and a relative dielectric

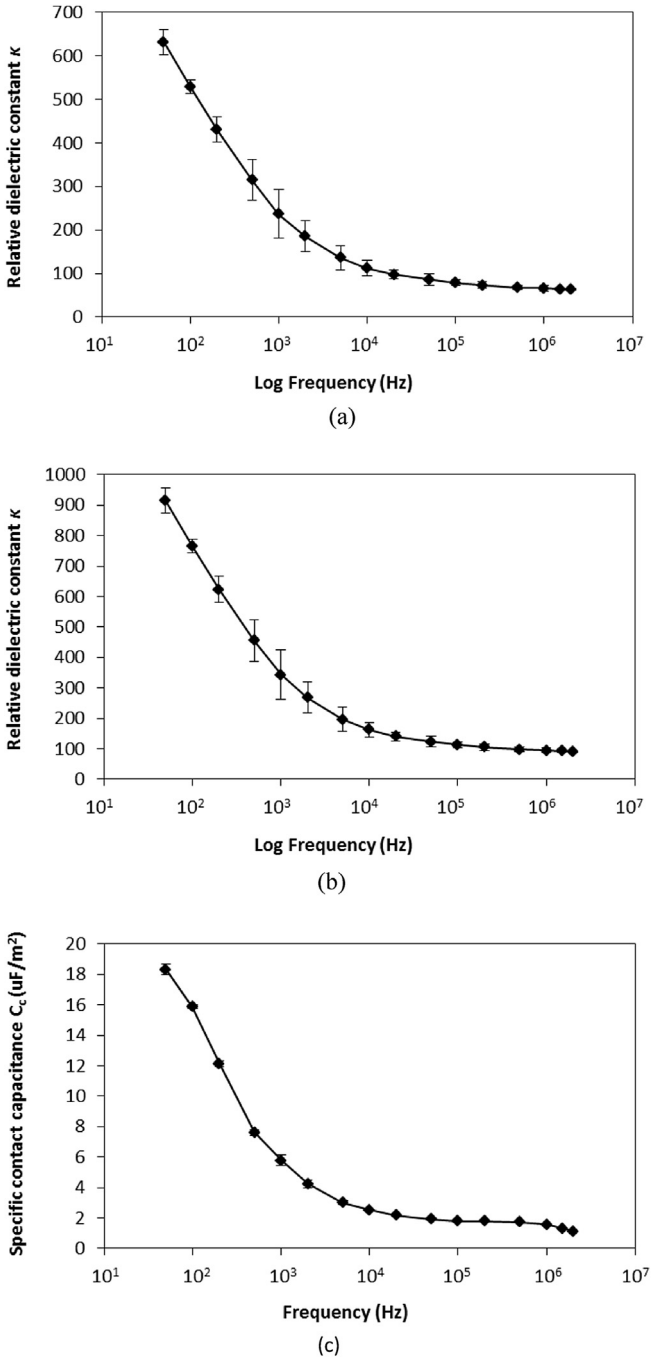

Fig. 4. (a) Plot of the through-thickness relative dielectric constant κ of the GO paper vs. the frequency. (a) The overall GO paper (with air included). (b) The solid part of the GO paper (with air excluded). (c) Plots of the through-thickness specific contact capacitance C_c between the solid part of the GO paper and the electrical contact vs. the frequency.

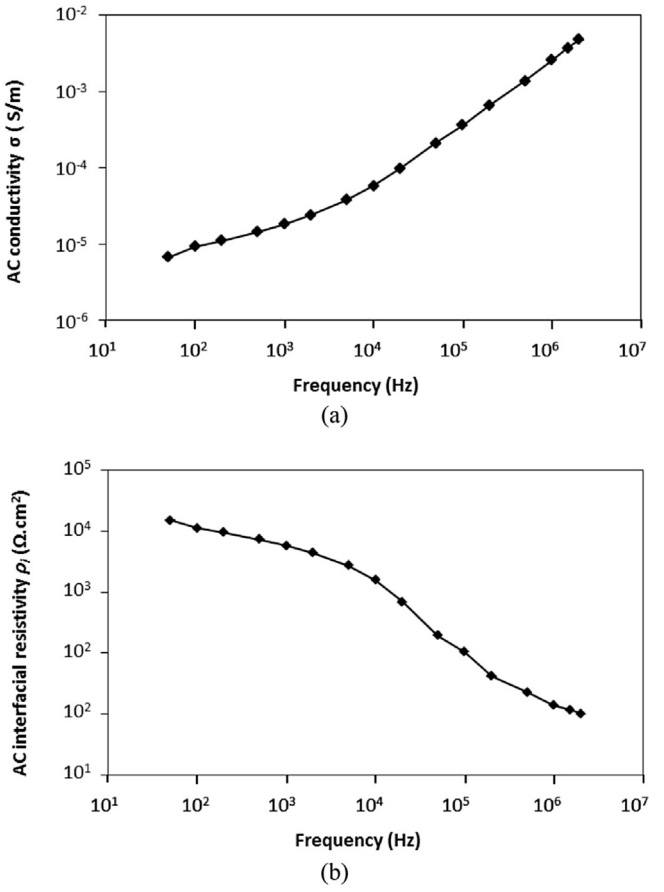

Fig. 5. (a) Plots of the through-thickness volume electrical conductivity σ of the solid part of the GO paper vs. the frequency. (b) Plots of the interfacial resistivity ρ_i between the solid part of the GO paper and an electrical contact vs. the frequency.

constant of 770 at 100 Hz and room temperature. The difference between the results of this work and those of prior work [14] is attributed to (i) the fact that the prior work uses the two-probe method and does not decouple the volumetric and interfacial contributions and (ii) the fact that the GO paper thickness is much smaller for the prior work (3 μm) than this work (221–559 μm). A smaller thickness enables a greater degree of preferred orientation of the carbon layers in the plane of the paper, thereby decreasing both the conductivity and the relative dielectric constant in the through-thickness direction.

The in-plane conductivity (Fig. 7(a)) increases with increasing frequency and is essentially independent of the thickness for the range of thickness studied. The increase with increasing frequency is less severe for the in-plane conductivity than the through-thickness conductivity (Fig. 5(a)). This is attributed to the difference in the effect of the interfaces in the material. The interface effect is small in the in-plane direction compared to that in the through-thickness direction, as expected from the preferred orientation of the carbon layers in the plane of the paper.

As shown in Fig. 7(a), the highest in-plane conductivity obtained for the solid part of the paper is 2.5 S/m. Fig. 7(b) shows that the ratio of the in-plane conductivity to through-thickness conductivity decreases with increasing frequency. This means that the degree of electrical anisotropy decreases with increasing frequency.

The GO has been widely considered to be an electrical insulator. This work shows that GO is conductive to a degree. Due to the greater degree of optical transparency of GO compared to graphene, the conductivity of GO makes this material potentially attractive for use as a transparent electrical contact material for solar cells and other optoelectronic devices, though the anticipated transmissivity would require a very small thickness. Compared to graphene or reduced GO, GO is more amenable to having their carbon layers separated.

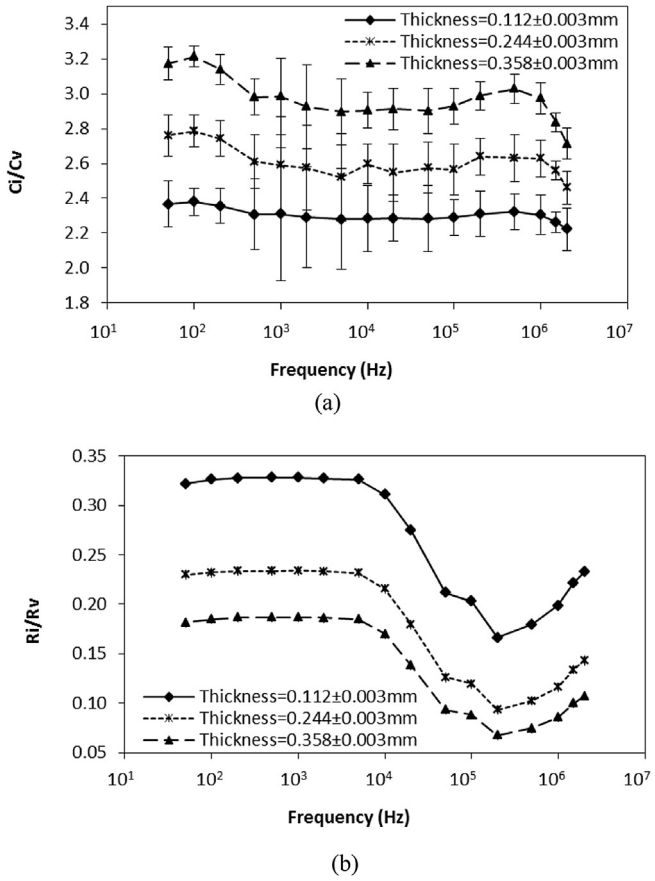

Fig. 6. The ratio of the contribution of the interface between the specimen and the electrical contact to the contribution of the volume of the specimen. (a) Capacitance. (b) Resistance.

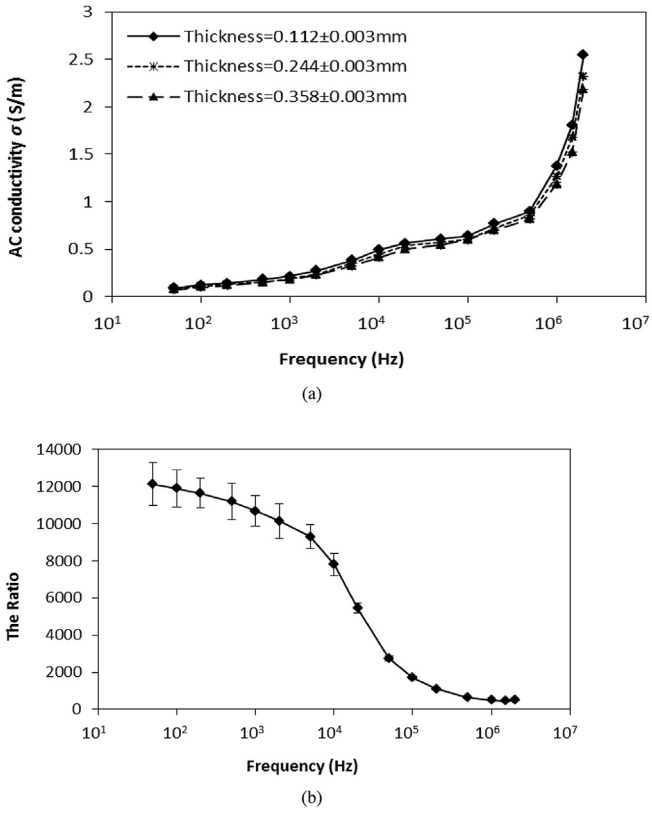

Fig. 7. (a) Plot of the in-plane conductivity of the solid part of the GO paper vs. the frequency, showing the effect of the paper thickness on the conductivity. (b) The ratio of in-plane conductivity to through-thickness conductivity of the solid part of the GO paper vs. the frequency. The in-plane values are those of the intermediate thickness of 0.244 ± 0.003 mm.

4. Conclusion

The GO paper (dark brown, with C/O atomic ratio 2.0 and interlayer spacing 8.6 Å) is found in this work to be a polarizable electrical conductor in the through-thickness direction. With unprecedented decoupling of the volumetric and interfacial contributions through the testing of paper of various thicknesses, the through-thickness dielectric and conduction properties have been determined, including the dependence of these properties on the frequency ranging from 50 Hz to 2 MHz.

The GO is prepared by using the modified Hummers method. In addition to the main XRD peak at 10° (interlayer spacing 8.6 Å), it has a weak XRD peak at 20 °C (interlayer spacing 4.3 Å), indicating incomplete intercalation, though there is no graphite 002 peak. The solid part of the GO paper amounts to 69.03 ± 0.25 vol% of the paper, with thickness ranging from 112 to 358 μm.

The solid part (69 vol%) of the paper exhibits in-plane electrical conductivity 0.07 and 2.5 S/m at 50 Hz and 2 MHz respectively, through-thickness conductivity 6.7×10^{-6} and 4.8×10^{-3} at 50 Hz and 2 MHz respectively, through-thickness relative dielectric constant κ 915 and 91 at 50 Hz and 2 MHz respectively, specific capacitance of the interface with an electrical contact 18.3 and 1.11 μF/m^2 at 50 Hz and 2 MHz respectively, and areal resistivity of this interface 1.5×10^5 and 1×10^2 Ω cm^2 at 50 Hz and 2 MHz respectively. The conductivity is due to slightly incomplete intercalation (but without residual graphite).

The significant decrease of κ with increasing frequency from 50 to 200 Hz is attributed to the dipole friction associated with the functional groups on the GO being sluggish in their response to the AC applied electric field. The increase of the conductivity with increasing frequency is attributed to the decreasing excursion of the charge carriers in a cycle as the frequency increases and the consequent decrease in the chance of the carriers to encounter an interface.

For the paper dimensions of this work, C_i is 2–3 times of C_v, and the ratio of R_i to R_v is below 0.35. This means that the paper-contact interface contributes substantially to both the measured capacitance and the measured resistance, though the paper capacitance and paper resistance (i.e., the volumetric quantities) dominate.

Acknowledgement

The authors thank China Scholarship Council (201406630067) for partial financial support of the first author.

References

[1] D.D.L. Chung, Carbon materials for structural self-sensing, electromagnetic shielding and thermal interfacing, Carbon 50 (9) (2012) 3342–3353.
[2] D.D.L. Chung, Carbon Composites, Elsevier, 2016. Ch. 1.
[3] D.P. Hansora, N.G. Shimpi, S. Mishra, Graphite to graphene via graphene oxide: an overview on synthesis, properties, and applications, JOM 67 (12) (2015) 2855–2868.
[4] Y. Zhu, S. Murali, W. Cai, X. Li, J.W. Suk, J.R. Potts, R.S. Ruoff, Graphene and graphene oxide: synthesis, properties, and applications, Adv. Mater Weinheim, Ger. 22 (35) (2010) 3906–3924.
[5] S.K. Srivastava, J. Pionteck, Recent advances in preparation, structure, properties and applications of graphite oxide, J. Nanosci. Nanotech. 15 (3) (2015)

1984–2000.
[6] Ronaldo Adriano Timm, Alexandre Kisner, Victor Costa Bassetto, Lauro Tatsuo Kubota, Critical view on graphene oxide production and its transfer to surfaces aiming electrochemical applications, J. Nanosci. Nanotech. 14 (9) (2014) 6478–6496.
[7] R.S. Sundaram, Chemically derived graphene, Wood Pub Ser. Electron Opt. Mater. 57 (2014) 50–98 (Graphene).
[8] Aihua Li, Jingquan Liu, Shengyu Feng, Applications of graphene based materials in energy and environmental science, Sci. Adv. Mater. 6 (2) (2014) 209–234.
[9] D.R. Dreyer, C.W. Bielawski, Graphite oxide as an olefin polymerization carbocatalyst: applications in electrochemical double layer capacitors, Adv. Funct. Mater. 22 (15) (2012) 3247–3253.
[10] D.W. Lee, J.W. Seo, G.R. Jelbert, L.V. L. de Los Santos, J.M. Cole, C. Panagopoulos, C.H.W. Barnes, Transparent and flexible polymerized graphite oxide thin film with frequency-dependent dielectric constant, Appl. Phys. Lett. 95 (17) (2009) 172901.
[11] M. Siyar, A. Maqsood, S.B. Khan, Synthesis of mono layer graphene oxide from sonicated graphite flakes and their Hall effect measurements, Mater Sci Pol. 32 (2) (2014) 292–296.
[12] P. Steurer, R. Wissert, R. Thomann, R. Mulhaupt, Functionalized graphenes and thermoplastic nanocomposites based upon expanded graphite oxide, Macromol. Rapid Commun. 30 (2009) 316–327.
[13] H. Shin, K.K. Kim, A. Benayad, S. Yoon, H.K. Park, I. Jung, M.H. Jin, H. Jeong, J.M. Kim, J. Choi, Y.H. Lee, Efficient reduction of graphite oxide by sodium borohydride and its effect on electrical conductance, Adv. Funct. Mater. 19 (12) (2009) 1987–1992.
[14] M. Yasin, T. Tauqeer, S.M.H. Zaidi, S.E. San, A. Mahmood, M.E. Kose, B. Canimkurbey, M. Okutan, Synthesis and electrical characterization of Graphene Oxide films, Thin Solid Films 590 (2015) 118–123.
[15] K. Zhang, Y. Zhang, S. Wang, Enhancing thermoelectric properties of organic composites through hierarchical nanostructures, Sci. Rep. 3 (2013) 3448.
[16] Y. Qian, A. Vu, W. Smyrl, A. Stein, 2012 Facile preparation and electrochemical properties of V_2O_5-graphene composite films as free-standing cathodes for rechargeable lithium batteries, J. Electrochem. Soc. 159 (8) (2012) A1135–A1140.
[17] H.K. Jeong, C. Yang, B.S. Kim, K. Kim, Valence band of graphite oxide, EPL Europhys. Lett. 92 (3) (2010), 37005 (4pp).
[18] X. Wang, T. Liu, Fabrication and characterization of ultrathin graphene oxide/poly(vinyl alcohol) composite films via layer-by-layer assembly, J. Macromol. Sci. Part B 50 (6) (2011) 1098–1107.
[19] H. Jeong, Y.P. Lee, R.J.W.E. Lahaye, M. Park, K.H. An, I.J. Kim, C. Yang, C.Y. Park, R.S. Ruoff, Y.H. Lee, Evidence of graphitic AB stacking order of graphite oxides, J. Am. Chem. Soc. 130 (4) (2008) 1362–1366.
[20] H. Jeong, H. Noh, J. Kim, M.H. Jin, C.Y. Park, Y.H. Lee, X-ray absorption spectroscopy of graphite oxide, EPL Europhys. Lett. 82 (6) (2008), 67004 (5pp).
[21] S. Mayavan, J. Sim, S.M. Choi, Simultaneous reduction, exfoliation and functionalization of graphite oxide into graphene-platinum nanoparticles hybrid toward methanol oxidation, J. Mater. Chem. 22 (2012) 6953–6958.
[22] Y. Wang, L. Tang, Z. Li, Y. Lin, J. Li, In situ simultaneous monitoring of ATP and GTP using a graphene oxide nanosheet–based sensing platform in living cells, Nat. Protoc. 9 (2014) 1944–1955.
[23] X. Qiao, S. Liao, C. You, R. Chen, Phosphorus and nitrogen dual doped and simultaneously reduced graphene oxide with high surface area as efficient metal-free electrocatalyst for oxygen reduction, Catalysts 5 (2) (2015) 981–991.
[24] M. Kole, T.K. Dey, Investigation of thermal conductivity, viscosity, and electrical conductivity of graphene based nanofluids, J. Appl. Phys. 113 (8) (2012) 084307.
[25] http://www.acsmaterial.com/product.asp?cid=120&id=155, as viewed on June 29, 2016.
[26] X. Hong, D.D.L. Chung, Exfoliated graphite with relative dielectric constant reaching 360, obtained by exfoliation of acid-intercalated graphite flakes without subsequent removal of the residual acidity, Carbon 91 (2015) 1–10.
[27] A. Wang, D.D.L. Chung, Dielectric and electrical conduction behavior of carbon paste electrochemical electrodes, with decoupling of carbon, electrolyte and interface contributions, Carbon 72 (2014) 135–151.
[28] D.D.L. Chung, A review of exfoliated graphite, J. Mater Sci. 51 (1) (2016) 554–568.
[29] W.S. Hummers Jr., R.E. Offeman, Preparation of graphitic oxide, J. Am. Chem. Soc. 80 (6) (1958), 1339–1339.
[30] S. Tankovich, D.A. Dikin, R.D. Piner, K.A. Kohlhaas, A. Kleinhammes, Y. Jia, R.S. Ruoff, Synthesis of graphene-based nanosheets via chemical reduction of exfoliated graphite oxide, Carbon 45 (7) (2007) 1558–1565.
[31] C. Bao, L. Song, C.A. Wilkie, B. Yuan, Y. Guo, Y. Hu, X. Gong, Graphite oxide, graphene, and metal-loaded graphene for fire safety applications of polystyrene, J. Mater. Chem. 22 (2012) 16399–16406.
[32] A. Lerf, A. Buchsteiner, J. Pieper, S. Schöttl, I. Dekany, T. Szabo, H.P. Boehm, Hydration behavior and dynamics of water molecules in graphite oxide, J. Phys. Chem. Solids 67 (5) (2006) 1106–1110.
[33] V.S. Channu, R. Bobba, R. Holzeca, Graphite and graphene oxide electrodes for lithium ion batteries, Colloids Surf. A Physicochem. Eng. Asp. 436 (2013) 245–251.
[34] T. Szabó, O. Berkesi, P. Forgó, K. Josepovits, Y. Sanakis, D. Petridis, I. Dékány, Evolution of surface functional groups in a series of progressively oxidized graphite oxides, Chem. Mater. 18 (11) (2006) 2740–2749.
[35] E. Fuente, J.A. Menendez, M.A. Diez, D. Suarez, M.A. Montes-Moran, Infrared spectroscopy of carbon materials: a quantum chemical study of model compounds, J. Phys. Chem. B 107 (26) (2003) 6350–6359.
[36] S. Stankovich, R.D. Piner, S.T. Nguyen, R.S. Ruoff, Synthesis and exfoliation of isocyanate-treated graphene oxide nanoplatelets, Carbon 44 (15) (2006) 3342–3347.
[37] H. He, J. Klinowski, M. Forster, A. Lerf, A new structural model for graphite oxide, Chem. Phys. Lett. 287 (1) (1998) 53–56.
[38] D.D.L. Chung, Carbon Fiber Composites, Butterworth-Heinemann, 1993.